







STAR Front-End Using Two Circulators in a Differential Connection

YINYI ZHAO ¹ (Student Member, IEEE), UDARA DE SILVA ¹ (Student Member, IEEE),
SATHEESH B. VENKATAKRISHNAN ¹ (Senior Member, IEEE),
DIMITRA PSYCHOGIOU ^{2,3} (Senior Member, IEEE), GROVER LARKINS ¹,
AND ARJUNA MADANAYAKE ¹ (Member, IEEE)

(Regular Paper)

¹Department of Electrical Engineering, Florida International University, Miami, FL 33174 USA

²Department of Electrical and Electronic Engineering, University College Cork, T12 K8AF Cork, Ireland

³Tyndall National Institute, T12 R5CP Cork, Ireland

CORRESPONDING AUTHOR: Arjuna Madanayake (e-mail: amadanay@fiu.edu).

The work of Arjuna Madanayake and Satheesh B. Venkatakrishnan was supported by NSF.

ABSTRACT In-band full duplex (IBFD) communication systems have attracted much interest due to their ability to double the spectrum efficiency by simultaneously transmitting and receiving (STAR) over the same bandwidth. Modern communication technologies have to adapt to be able to meet the ongoing high demand capacity over existing radio channels. This paper proposes a system-level approach based on physical symmetry to improve the electromagnetic performance of a 3-port circulator. A system-level design consisting of two matched circulators connected in a differential configuration is proposed to cancel out residual RF scattering and leakage that causes self-interference in a STAR front-end. The method is validated using a custom designed microwave circulator based on microstrip technology, which forms a building block that operates in the 3–8 GHz band with 20 dB isolation. The proposed RF front-end operates within an extended band of 3–8 GHz while simultaneously exhibiting improvement in isolation by about 10 dB (isolation 30 ± 4 dB) between the transmitter and the receiver ports of the STAR system.

INDEX TERMS IBFD, STAR, SIC, ferrite, circulator, wide bandwidth, high isolation, sub-6 GHz, full duplex system, microstrip.

I. INTRODUCTION

There is severe crowding in the sub-6 GHz “legacy” bands, where bandwidth is at a premium for terrestrial and space services. The FR1-band, which is the band up to 6 GHz in the radio spectrum, is extremely important to many stakeholders and spectral resources in this band are at a premium. Although mm-wave spectrum is abundant and the future of wireless relies on moving many services to mm-wave bands, legacy FR1-band frequencies remain extremely important for communications due to the favorable physics for highly-scattering urban environments (e.g., low path-loss). As a consequence, there is, and always will be, a strong demand for the sub-6 GHz spectral band from both commercial, public safety, and military systems. For example, the air interface standard for 5G cellular (known as 5G NR) includes multiple sub-6 GHz bands (0.6–0.7 GHz, 3.3–3.8 GHz, etc.) [1]. Full duplex

(FD) radios can simultaneously transmit and receive (STAR) two information-carrying signals over the same bandwidth (in-band). The adoption of in-band FD wireless effectively doubles the bandwidth of operation and the capacity of the wireless channel for a given signal to noise ratio (SNR). Such a doubling of capacity is a tremendous advantage for wireless communications in legacy spectral bands. In addition to capacity increases from a communications standpoint, STAR provides the ability for joint communications and sensing within the same frequency band.

To increase the channel capacity, we can either increase the bandwidth or the SNR. However, the fundamental issue of in-band full-duplex (IBFD) system is the inherent self-interference (SI) present at the STAR receiver. SI is caused by the leakage that occurs directly from the Tx to Rx. This results in a degradation of the performance of the system and reduces

the channel capacity due to very high levels of interference. To combat this problem, self-interference cancellation (SIC) is required in the IBFD system to increase the SNR and, by extension, the capacity of the channel. This paper discusses radio frequency (RF) front-end designs for IBFD wireless applications based on the system level design using ferrite circulators. Ferrite circulators are capable of reasonable power handling and offers low noise and high linearity. We focus on system level innovations that do not include integrated circuit (IC) realizations of circulators, which are beyond the scope of this paper.

The rest of the paper is organized as follows. Section II contains a review of the literature pertaining to full duplex front-end approaches including ferrite circulators, balanced duplexers, and multiple circulator approaches for STAR. Section III introduces the proposed architecture for full duplex front-ends using two ferrite circulators. This section covers ferrite circulator design aspects and COMSOL Multiphysics based simulation of a two circulator front-end STAR system. Section IV covers the fabrication, measurement and evaluation of the proposed two circulator architecture leading to measured performance plots. Finally, in Section V the paper is concluded.

II. REVIEW OF STAR FRONT-ENDS

We reviewed existing approaches and their achievable cancellation, and compared them with our proposed SIC technique in the following section. In most cases, shared aperture STAR (SA-STAR) architecture either uses balanced duplexers or circulators to realize full-duplex operation [2]. Circulators are building blocks for full-duplex transceivers as it allows STAR operation within the same band of interest. SA-STAR using an electrical balanced duplexer (EBD) has more losses and degraded noise figures compared to circulator-based SA-STAR [2]. On the contrary, circulator-based SA-STAR provides both lower losses and improved noise figures, at the cost of narrowband operation. Furthermore, EBD approaches to STAR can be categorized as active or passive; circulators can be classified as based on either magnetic and nonmagnetic principles of operations [2]. Different static or dynamic (i.e., adaptive) approaches exist for using EBD and circulators in SA-STAR radio.

A. BALANCED DUPLEXER-BASED SA-STAR

A duplexer permits bi-directional communication over a single path. This costs at least 3 dB of loss for a transmitted signal and a 3 dB degradation of the receiver noise floor. This is due to the balancing as well as the equal splitting of the losses between the Tx-Rx chain [3]. Table I enumerates the design properties for the balanced duplexer-based SA-STAR. Based on the operation principle of balanced duplexers in SA-STAR radios, it can be of the following types:

Single/Differential Balanced duplexer: Existing single-balanced architecture is able to provide 60 dB of isolation for 50 MHz bandwidth by exploiting the differential mode (DM) excitation only at the transmitter end [3]. However, this

TABLE 1. Review on Balanced Duplexer-Based SA-STAR

Reference	Technology	Isolation (Max) (dB)	Center Frequency (GHz)	Bandwidth (GHz)
[3]	electrical balanced duplexer	62	1.9	0.020
[4]	tunable electrical balanced duplexer	50	2.4	0.070
[5]	tunable electrical balanced duplexer	53	1.9	0.050
[8]	0.18um SOI CMOS	50	0.85	0.010
[9]	0.18um SOI CMOS	60	0.85	0.3
[11]	Discrete electrical balanced duplexer	53.4	2.45	0.080

approach lacks the common mode (CM) isolation required to protect the LNA from saturation [3]. It is possible to protect LNA from saturation by extending the differential mode to be symmetric; however, this comes at the expense of increased noise floor of the receiver due to the addition of baluns and the requirement of an auxiliary transmit chain.

Tunable balanced duplexer: Unlike static balanced duplexers, tunable EBD tune the balance load to match the antenna impedance better. This tunability minimizes the in-band self-interference and ensures high isolation between the Tx-Rx chain. An automated tuning algorithm was reported to have 45 dB of isolation at the 2.4 GHz ISM band [4]. Another experimental demonstration reported having a 60 dB of isolation across 50 MHz bandwidth [5].

Adaptive balanced duplexer: An adaptive balanced duplexer is required to cancel self-interference in real-time. This adaptation is required to deal with reflected path SI components in a dynamic wireless environment [6]. In a dynamic wireless environment, a swarm optimizer uses adaptive multi-bit tunable capacitor banks to deal with self-interference within 1 ms [7]. This multi-bit, multi-path architecture can provide 40–50 dB of isolation across 1.5–3.5 MHz bandwidth in a dynamic wireless environment [8], [9]. A real-world demonstration was reported to achieve a greater than 50 dB isolation across a 20 MHz bandwidth within a 5 ms tuning cycle [10]. Further, a digitally aided EBD provided 53 dB of Tx-Rx isolation and enhanced the performance across a larger bandwidth of 80 MHz in the ISM band [11].

B. CIRCULATOR-BASED SA-STAR

The main advantage of using circulators over EBD is that they do not suffer from the 3 dB insertion loss associated with EBD. A circulator can be designed using either hybrid couplers or transistors, while in nature, it can be either magnetic or nonmagnetic. Table II lists the design properties for the circulator-based SA-STAR. The following section will

TABLE 2. Review on Circulator-Based SA-STAR

Reference	Technology	Connection type	Tx-Ant loss _{Min} (dB)	Ant-Rx loss _{Min} (dB)	Isolation _{Max} (dB)	Center Frequency (GHz)	Bandwidth (GHz)	NF (dB)	OOB IIP3 (dBm)	IB IIP3 (dBm)
[12]	Microstrip ferrite	Discrete	N/A	N/A	39.5	2.45	0.065	N/A	N/A	N/A
[13]	Microstrip ferrite	Discrete	N/A	N/A	60	8.5	0.8	3	N/A	N/A
[14]	LTI AlN MEMS	Integrated	11	N/A	15	1.168	0.0022	N/A	N/A	N/A
[15]	65nm CMOS	Integrated	N/A	N/A	50	0.7	0.032	5	+19	-33
[16]	65nm CMOS	Integrated	3.1	N/A	40	0.73	0.056	2.7	+14	-4
[17]	180nm SOI CMOS	Integrated	2.1	2.9	25	0.97	0.215	3.1	N/A	N/A
[18]	45nm SOI CMOS	Integrated	3.3	3.2	18.5	25	4.6	4	+19.9	N/A
[19]	SSDL GaN MMIC	Discrete	8	9	25	1.5	1	N/A	N/A	N/A
[20]	Microstrip	Discrete	7	7	32	0.5	1	N/A	N/A	N/A
[21]	0.25um pHEMT	Integrated	4.5	4.5	35	11.5	2.6	4.5	N/A	N/A
This work	Microstrip ferrite	Discrete	8	5	32	4.5	7	N/A	N/A	N/A

describe the operation principle and the recent advancement in magnetic/nonmagnetic circulator-based SA-STAR radios.

Magnetic Circulator: Three port magnetic circulator exploits wave propagation and cancellation based on the Faraday effect on magnetic/ferrite cores having limited narrowband isolation [12]. This limited isolation can be enhanced by improving the impedance matching through the use of varactor diodes which act as a reconfigurable impedance match terminal (IMT). Existing work showed the cancellation of 40 dB across a 65 MHz bandwidth at 2.45 GHz [12]. This aforementioned magnetic circulator-based SA-STAR radio has a narrow bandwidth. Broadband isolation requires multiple ferrite circulators and couplers arrangement, resulting in a larger footprint. A multi section Lange-couplers and ferrite circulator design arranged in a symmetric fashion has been shown to realize a 60 dB of isolation across an 800 MHz bandwidth [13].

Non-Magnetic Circulator: An alternative way to realize a nonmagnetic circulator is by using a transmission line with periodically spaced transistor-based switches. Combined with a quarter wavelength arrangement, variable phased-clock-driven transistors can be used to emulate the operation of a circulator operation [14]. Most importantly, this concept can be implemented in an integrated circuit using N-path filters and switches [15], [16]. Implementations using a CMOS integrated circuit showed 15 dB of isolation across a 2.2 MHz bandwidth [15]. Additionally, N-path filters were integrated with the CMOS process and attained 50 dB of remarkable isolation across a 32 MHz bandwidth [15]. Other work reported achieving 40 dB of isolation across a 56 MHz bandwidth, while maintaining a 2.7 dB receiver noise figure [16].

Recently, researchers demonstrated a significant contribution to realizing compact integrated nonmagnetic high isolation circulator-based SA-STAR front end [17] operating at mm-wave [18]. Further, wideband isolation ranging

from 20–35 dB was reported in [19], [20], where they used a novel sequentially-switched delay line (SSSDL) to realize nonmagnetic circulator-based SA-STAR radio. Further, an ultrawideband 2.5 GHz SA-STAR radio was realized with 35 dB of isolation by combining three quadrature hybrids [21].

III. PROPOSED FERRITE-BASED 2-CIRCULATOR STAR FRONT-END

The IBFD communication system is interesting due to its ability to double the spectral efficiency by STAR. As there is a rapid development of communication technologies and there is a resulting demand of high traffic levels over existing channels, a considerable expansion of the capacity of the communication channels is required using available FR1 (sub 6 GHz) bands without additional spectral allocations. According to the Shannon-Hartley law, the capacity, in bits per second, can be expressed as $C_c = W \log_2(1 + SNR)$ where W is the bandwidth of the channel in hertz and SNR refers to the signal to noise ratio in linear [22].

A circulator is a non-reciprocal microwave component that allows STAR from a single antenna. Real-world circulators must provide adequate isolation between the transmitter and the receiver despite mismatches to the antenna, transmitter and receiver, across the potentially wide operation. Ferrite circulators are typically narrowband, and furnish a complex-valued and highly frequency dependent driving point characteristic across a wideband region of the frequency spectrum. For example, the sub-6 GHz band is desirable for emerging full-duplex STAR applications, but the demands on matching and isolation across this band for real-world circulators are difficult to achieve due to the frequency dependence of the designs and materials.

From a microwave circuit design standpoint, a circulator can be thought of as a 3-port device having scattering (S-) parameters given by (1), and (2) for ideal and real-world cases

TABLE 3. Performance Comparison of Published Single Circulators

Reference	Technology	Tx-Ant loss $_{Min}$ (dB)	Ant-Rx loss $_{Min}$ (dB)	Isolation $_{Max}$ (dB)	Center Frequency (GHz)	Bandwidth (GHz)	Metric M_1	Metric M_2
[26]	Microstrip	2.7	2.7	44	30.5	0.2	164.7	34.9
[27]	Microstrip	0.4	0.1	20	9.6	1.2	12.5	4.0
[29]	Microstrip	0.51	0.51	33	4.25	1.1	516.4	158.9
[30]	Microstrip	3	3	9	4.3	0.6	1.1	0.22
[31]	Microstrip	0.5	0.5	20	12	4	33.3	10.3
[32]	Stripline	9	9	15	1.8	0.4	7.0	0.4
[33]	Stripline	0.75	0.75	21	4.6	1.2	32.8	9.7
[34]	Stripline	0.37	0.37	25	7.5	7	295.1	92.9
[35]	Stripline	1.5	1.7	28	0.3	0.2	420.6	108.1
[36]	Microstrip	0.4	0.4	23	0.6	0.4	133.0	41.7
[37]	Microstrip	2.7	4.5	20	3	0.2	6.7	1.2
This work	Microstrip	3	3.5	30	5.5	4.6	836.4	159.8

respectively, where $|\gamma| \leq 1$ represents small imperfections due to impedance mismatch/variations [23].

$$S_{Ideal} = \begin{bmatrix} 0 & 0 & 1 \\ 1 & 0 & 0 \\ 0 & 1 & 0 \end{bmatrix} \quad (1)$$

$$S_{Real-World} \approx \begin{bmatrix} \gamma & \gamma & 1 - \gamma^2 \\ 1 - \gamma^2 & \gamma & \gamma \\ \gamma & 1 - \gamma^2 & \gamma \end{bmatrix} \gamma \in \mathbb{C} \quad (2)$$

A. FERRITE-BASED MICROSTRIP CIRCULATORS

Ferrite-based microstrip circulators exhibit a narrow frequency range of operation typically in the range 600–800 MHz [24], [25], [26], [27], [28]. Due to emerging requirements for circulators to operate within a wider frequency range, ideally covering the legacy band, some frequency broadening techniques have been proposed in the literature. The studies in [29] and [30] explored the effect the “fill factor” of the ferrite has on the bandwidth, enabling optimization of frequency range via modification of the thickness of the ferrite puck inserted in the circulator cavity; this technique has been shown to achieve around 1.6 GHz bandwidth. Moreover, the study in [30] further explored the effect of DC magnetic bias field and impedance matching on the optimization of the circulator bandwidth. By properly placing the ferrite, the study in [31] shows the bandwidth broadening via low-temperature co-fired ceramics (LTCC) and sintered bulk ferrites.

Another optimization on the Y-shape conductor of the stripline circulator has been proposed in [32], [33], [34] to achieve a broad bandwidth. Impedance matching structures via lumped elements for the microstrip circulator were deployed in [35], [36], [37]. However, applying lumped elements to achieve impedance matching for a microstrip based

circuit design is not an optimal choice. Thus, impedance matching via microstrip transformers were attempted. The study in [30] introduces the stepped impedance matching network. Papers [38] and [39] present a detailed analysis of the impedance matching via network theory where it was concluded that the bandwidth can be broadened as long as the port impedance is within a prescribed range. However, the figures in these publications only show the circulator design without the impedance matching network, a detailed illustration or photos on their fabricated impedance matching network was not provided. Further to this, [31], [38] and [39] reports a bandwidth over 5 GHz at X-band. The design properties for the ferrite based circulator are specified in Table III. As numerous design properties, such as minimum forward loss, maximum isolation, center frequency, and the bandwidth, we use a metric $M_1 = I/Q$ [2], and also introduce a new metric M_2 which is defined in (3).

$$M_2 = \frac{I}{(1 + L_1 + L_2)Q} \quad (3)$$

Where I is the maximum isolation, $Q = F/B$, where F is the operating central frequency in GHz, and B refers to the bandwidth in GHz, and where L_1 is the loss from the Tx to the Antenna port in the circular, and L_2 is the average from the Antenna port to the Rx port in the circulator (isolation and losses are in dB). The proposed metric M_2 is designed to improve upon M_1 by taking into account the forward losses in the circulator that impacts system power efficiency and noise figure of the receiver. Both metrics are equivalent for the case of a lossless circulator. The M_2 metric aims to define a system-level equivalent of M_1 , which would indeed provide a design spec guideline for the STAR front-end based on two differentially connected circulators reported in this manuscript.

TABLE 4. Properties of Different Ferrite Materials

Type number	Saturation Magnetization $4\pi M_s$ (Gauss)	Line width Δh Oe	Dielectric Constant
TT1-105	1750	≤ 270	12.2
TT2-111	5000	≤ 200	12.9

B. FERRITE CIRCULATOR DESIGN EQUATIONS

One important parameter for the ferrite based circulator is the radius of the ferrite puck, which can be calculated by (4) [40].

$$kR = x \quad (4)$$

$$k = (\omega/c)\sqrt{(\mu_{eff} \cdot \epsilon_f)} \quad (5)$$

In (4), R is the radius of the ferrite cylinder, k is the wave propagation constant that is found via (5) where the parameter x corresponds to the *first circulation condition*, which in turn is typically found to be $x = 1.841$ [40], and the resonance at $\omega = 2\pi f$ in radians/second, where f is the resonant frequency in Hz, and $c = 3 \cdot 10^8$ m/s is the speed of light, and μ_{eff} is the effective permeability of the ferrite cylinder, given by (6) [40].

$$\mu_{eff} = (\mu^2 - k^2)/\mu \quad (6)$$

We recall that quantities μ and k are polder tensor elements of the ferrite cylinder which can be calculated through (7) and (8) [40].

$$k = -\frac{f_m f}{f_z^2 - f^2} \quad (7)$$

$$\mu = 1 + \frac{f_m f_z}{f_z^2 - f^2} \quad (8)$$

Where f is the frequency of operation, $f_m = 2.8 \times 4\pi M_s$ MHz, M_s is the saturation magnetization, $f_z = 2.8H_0$ MHz, H_0 is the applied magnetic field in Oe.

1) COMPUTER SIMULATION USING COMSOL

The selection of the correct ferrite material is important for optimum performance of a circulator. Higher levels saturation magnetization will result in a wider bandwidth at the cost of reduced power handling capability [27]. Table IV lists two types of ferrite material; for our designs, the ferrite of type TT2-111 was selected in order to obtain a larger saturation magnetization resulting in also achieving a wide bandwidth.

The frequency performance of the circulator depends on magnetic properties of the ferrite material. To simulate the nonlinear effects in a ferrite, we used the simulation tools from COMSOL Multiphysics. The definition of the anisotropic permeability of a ferrite magnetized in the positive z -direction as defined in COMSOL Multiphysics modeling environment

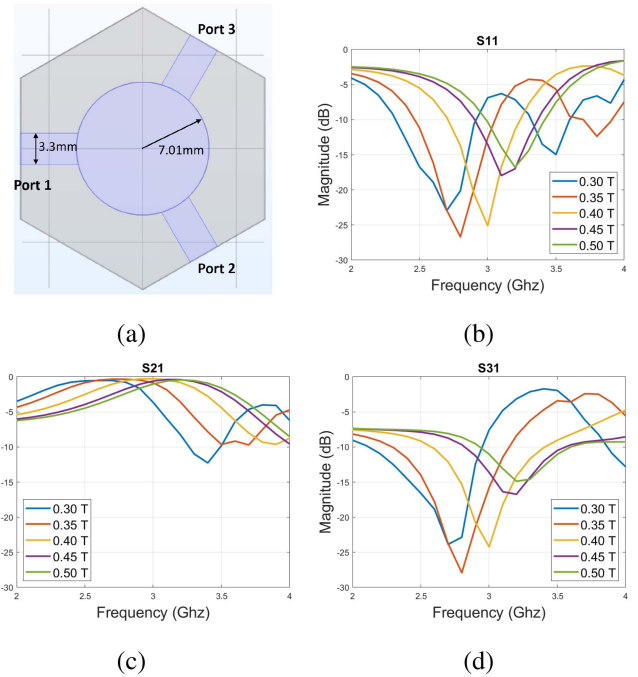


FIGURE 1. Ferrite circulator design without the matching network: (a) Circulator geometry. (b) Return loss. (c) Insertion loss. (d) Isolation.

is expressed in (9) [41]:

$$[\mu] = \begin{bmatrix} \mu & j\kappa & 0 \\ -j\kappa & \mu & 0 \\ 0 & 0 & \mu_0 \end{bmatrix} \quad (9)$$

where

$$\kappa = \mu_0 \frac{\omega\omega_m}{\omega_0^2 - \omega^2} \quad (10)$$

$$\mu = \mu_0 \left(1 + \frac{\omega\omega_m}{\omega_0^2 - \omega^2} \right) \quad (11)$$

$$\omega_0 = \mu_0(\gamma H_0) \quad (12)$$

$$\omega_m = \mu_0(\gamma M_s) \quad (13)$$

In (10)–(13), μ_0 denotes the permeability of free space, ω is the angular frequency, ω_0 is the Larmor frequency of a spinning electron in the applied magnetic bias field shown as H_0 , and ω_m is the electron Larmor frequency at the saturation magnetization of the ferrite M_s , and γ is the gyromagnetic ratio of the electron [41].

Applying (4) to (8), for an operating frequency of 3 GHz, the radius of the cylinder is $R = 7.01$ mm. The substrate is Rogers 4350B having $\epsilon = 3.48$ and thickness $h = 1.524$ mm. To achieve a 50Ω characteristic impedance, the width of the microstrip line was determined to be 3.3 mm. The applied magnetic bias field in the simulation was varied from $H_0 = 0.3$ T to 0.5 T (3000 Gauss to 5000 Gauss). The simulation

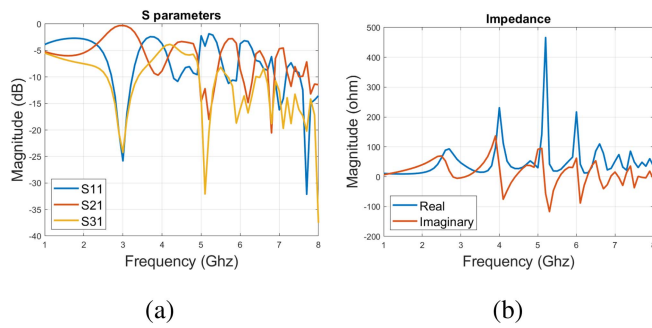


FIGURE 2. Ferrite circulator without the matching network simulation result (Port 1 as the excitation): (a) S-parameters. (b) Impedance.

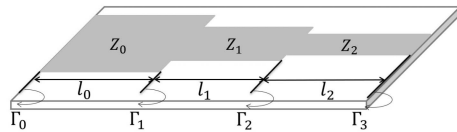


FIGURE 3. Three-section microstrip Chebyshev matching transformer.

geometry of the circulator design is shown in Fig. 1(a), and the corresponding simulation results are shown in Fig. 1(b)–(d).

The COMSOL simulation shows that the s-parameter curve shifts from low to high frequency when increasing the magnetic bias field, and the optimal performance for the designed 3 GHz operation frequency can be achieved by applying a biased field of 0.4 T (4000 Gauss). Thus, the applied magnetic bias field for the following simulation is selected to be $H_0 = 0.4$ T, the gyromagnetic ratio γ is 1.759×10^{11} C/kg; The permittivity of free space ϵ is 8.85×10^{-12} F/m, and the permeability of free space μ_0 is 1.26×10^{-6} H/m. Fig. 1(c) and (d) indicate that the designed circulator can operate from 2.8 to 3.4 GHz in a counterclockwise direction with low insertion loss and the isolation between ports is approximately 23 dB. However, as shown in Fig. 2(a), the circulator is not operating at other frequencies since the impedance only matches to 50 Ω at the frequency of 3 GHz, which is shown in Fig. 2(b), making the operational band rather narrow. Therefore, wideband impedance matching networks are included in the design.

C. WIDEBAND IMPEDANCE MATCHING TO CIRCULATOR PORTS

Chebyshev multi-section matching transformers are applied as the matching network prototype due to their broadband matching properties. One three-section Chebyshev matching transformer is shown in Fig. 3, where Γ_n ($n = 1, 2, 3$) denotes the reflection coefficient, which is defined using (14) [42]:

$$\Gamma_n = \frac{Z_{n+1} - Z_n}{Z_{n+1} + Z_n} \quad (14)$$

Prior to wideband impedance matching, a specific value of the port impedance for matching the 50 Ω is required. In [38] and [39], it was shown that the real part of the circulator's

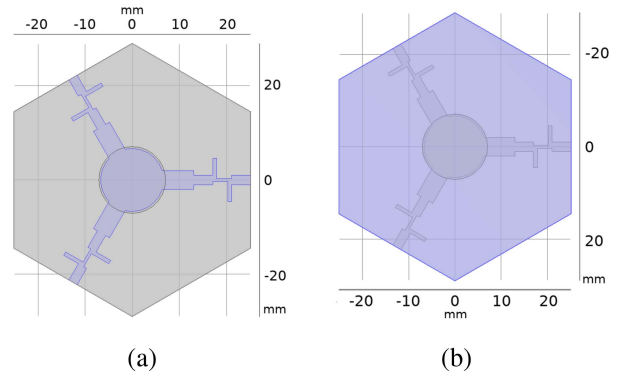


FIGURE 4. Ferrite circulator design with the matching network: (a) Top conductor of the circulator. (b) Bottom ground of the circulator.

impedance should remain in the range 10 to 70 Ω for appropriate operation, and the imaginary part of the circulator's impedance should keep between -50 to 50 Ω . Fig. 2(b) shows that the real part of the port impedance varies from 10 to 200 Ω , therefore, 100 Ω is selected for the prototype to match a 50 Ω load. Assuming the maximum allowable reflection coefficient Γ_m is 0.05, θ_m is 44.7° according to (15), where $N = 3$; Γ_0 and Γ_1 can be derived following the models in (16) [42]:

$$\sec\theta_m = \cosh\left(\frac{1}{N} \operatorname{arccosh}\left(\frac{\ln Z_L/Z_0}{2\Gamma_m}\right)\right) \quad (15)$$

$$2(\Gamma_0 \cos 3\theta + \Gamma_1 \cos \theta) = \Gamma_m \sec^3 \theta_m (\cos 3\theta + 3 \cos \theta) - 3\Gamma_m \sec \theta_m \cos \theta \quad (16)$$

$$\ln Z_n = \ln Z_{n-1} + 2\Gamma_{n-1} \quad (17)$$

From symmetry, it follows that $\Gamma_0 = \Gamma_3 = 0.0698$ and $\Gamma_1 = \Gamma_2 = 0.1037$. The required impedance Z_n for each section can be calculated employing (17) [42], which results in $Z_1 = 57.5$ Ω , $Z_2 = 70.7$ Ω and $Z_3 = 87$ Ω . To achieve better performance, two open stubs are introduced to achieve further impedance optimization. Considering the magnetic field at the near edge of the ferrite punk is not uniform, the radius of the circular copper conductor effectively “shrinks” slightly down to 6.63 mm. Meanwhile, [31] shows that by keeping the copper conductor marginally smaller than the ferrite cylinder, the operating bandwidth can be further increased. In [29], [31], [37] it was shown that by changing the fill factor, the bandwidth performance can be further improved.

Through the optimization procedure, the ultimate ferrite circulator design with wideband impedance matching is shown in Fig. 4. The thickness of the fabricated ferrite cylinder is 0.424 mm (TT2-111 from Island Ceramic Grinding Inc.). Fig. 5 shows the COMSOL Multiphysics simulation results of the s-parameters and the port impedance by applying the same optimal magnetic bias field (0.4 T). Compared with

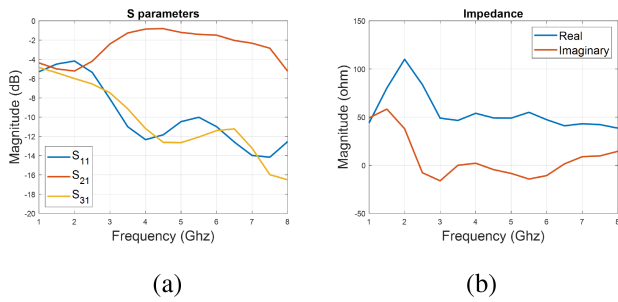


FIGURE 5. Ferrite circulator with matching network simulation result (Port 1 as the excitation): (a) S parameters. (b) Port impedance.

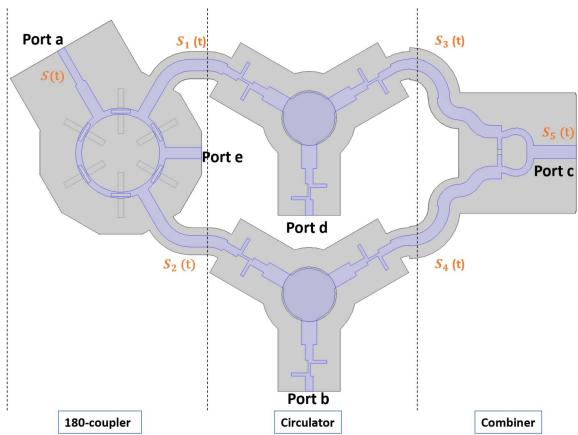


FIGURE 6. Proposed IBFD system model in COMSOL Multiphysics. The corresponding measurement results are shown in Fig. 10.

the impedance before matching, which is shown in Figs. 2(b), 5(b) shows that the real part of the impedance within the band of interest running from 3 to 7 GHz maintains within 30 to 80 Ω , and the imaginary part of the impedance maintains within -20 to 20 Ω after adding the impedance matching network and optimization. Therefore, the optimized circulator can achieve a wide bandwidth from 3 to 7 GHz as shown in Fig. 5(a). The insertion loss of the circulator is within 1 to 4 dB from 3 to 7 GHz after optimization, and the isolation is around 16 dB. The magnetic field in the commercially sourced rare earth magnet was measured, and was found to be 0.3988 T which is close to the target value.

D. DESIGN OF THE SIC ARCHITECTURE

The proposed SIC architecture, depicted in Fig. 6(a), contains one 180° coupler, two identical circulators, and one power combiner. Since the circulator operates at the counterclockwise direction, port *a* is the Tx port of the transmitter, port *b* and port *d* are the antenna output ports, port *c* is the Rx port of the receiver, and port *e* is the isolated port of the coupler. The scattering matrix for a ideal 3 dB 180° coupler can be

expressed in (18) [42]:

$$[S] = \frac{-j}{\sqrt{2}} \begin{bmatrix} 0 & 1 & 1 & 0 \\ 1 & 0 & 0 & -1 \\ 1 & 0 & 0 & 1 \\ 0 & -1 & 1 & 0 \end{bmatrix} \quad (18)$$

Thus, assuming the transmit signal at port 1 is $S(t)$, the two output of the coupler $S_1 = \frac{1}{\sqrt{2}}S(t) \angle -90^\circ$, and $S_2 = \frac{1}{\sqrt{2}}S(t) \angle -270^\circ$. Likewise, the leakage signals from the circulators $S_3(t)$ and $S_4(t)$ also have 180° in phase. At the combiner, the combined signal $S_5(t) = S_3(t) + S_4(t)$ will be small valued since $S_3(t)$ and $S_4(t)$ cancel each other. Although the optimized circulator design can achieve a broadband performance, the overall system's bandwidth is still being constrained, and that is caused by the conventional microstrip rat-race coupler and microstrip Wilkinson power divider which are narrow-band performance elements.

E. COMPUTER SIMULATIONS

The SIC simulation model after the optimization is shown in Fig. 6(a) by using COMSOL Multiphysics. The substrate used in the simulation is 1.52 mm thickness RO4350B with $\epsilon = 3.48$. In the system structure, which is shown in Fig. 6(a), the left side component is one 180° rat-race coupler to split the signal into two signals with 180° phase difference, the right side components consists of a Wilkinson power combiner and two identical circulators that are placed between the coupler and power combiner. Port *d* and port *e* are terminated with 50 Ω , and all other ports are connected with 50 Ω ports in the simulation.

The overall system performance is constrained by the designed microstrip coupler and microstrip power combiner. The simulated s-parameters from 1 to 8 GHz are shown in Fig. 6(b) to (e). Since the designed coupler and power combiner only have 2 GHz bandwidth from 3 to 5 GHz, the FD system also works between that range. At the Tx side, the insertion loss S_{ba} of the simulated FD system is around 5 dB since the coupler will introduce an additional about 3 dB loss and the circulator has around 2 dB intrinsic loss. At the Rx side, the minimum insertion loss S_{cb} is around 5 dB, and the maximum isolation from port *b* to port *a* is around 28 dB. By using two identical circulators in two symmetrical signal paths leads to the combined leakage interference signal at the Rx port *c* to undergo destructive interference and thereby significantly reduce in power compared to their usual case of using a single circulator. The scattering behavior due to impedance mismatches across the 1–8 GHz also largely cancel out causing an increased bandwidth compared to that of a single circulator.

IV. EXPERIMENTS

A. MEASUREMENT OF A SINGLE CIRCULATOR

RO4350B with a 1.52 mm substrate thickness and 35 μm copper thickness from Rogers Corporation was selected for

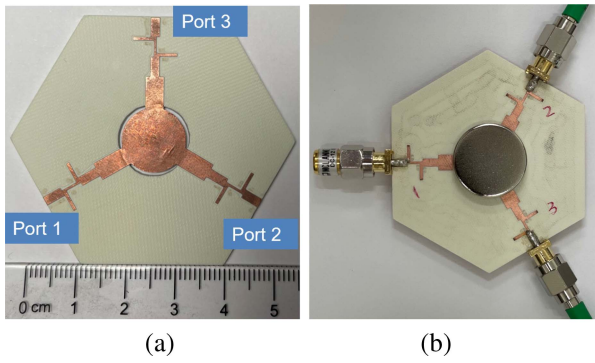


FIGURE 7. Proposed circulator design: (a) Copper conductor. (b) Circulator with ferrite inserted and magnets.

the substrate, and TT2-111 magnetic ferrite was selected for the magnetic ferrite puck material. The fabricated prototype circulator is shown in Fig. 7. Fig. 7(a) shows the circulator’s (top side) copper conductors, where the middle circle of the copper conductor is slightly smaller than the via hole on the substrate - also used to insert the ferrite puck. Fig. 7(b) depicts the circulator with ferrite inserted and magnets for measurement.

1) MEASURED MAGNETIC FIELD

A magnetic field probe (TD8620 from HFBTE) was used to experimentally verify the magnetic field bias for the ferrite core. The upper side magnet is placed above the copper conductor, and one small piece of plastic is placed between the magnet and the substrate to adjust the magnetic field. The magnetic field was measured to be 0.3933 T, which is close to the value in the simulation.

2) MEASURED S-PARAMETERS

A magnetic field of around 0.4 T that is close to the COMSOL simulation can be generated by using two DC2-N52 magnets. The measured results indicate that DC2-N52, where 3933 Gauss magnetic field applied to the circulator, achieves the best performance while other magnetic fields cannot make the circulator operate at higher performance levels. Thus, DC2-N52 is used to generate the magnetic field in the following measurements. Fig. 8(a) to (c) denote that the designed circulator operates between 3.5 to 8 GHz can achieve maximum high isolation 25 dB to 35 dB.

The measured return loss of the circulator is shown in Fig. 8(d). The insertion loss is a marginally larger than the simulation results which probably due to fabrication errors and deviations in material properties of their ideal valued used in the COMSOL model. Moreover, in the COMSOL environment, there is no gap between the ferrite puck and the conductor; however, in the reality, there do exist some gap between the puck and the copper conductor due to the raw fabrication accuracy. The model in the COMSOL is more like an ideal version compared to the reality model. Therefore, some properties such as the uniform of magnetic field and material

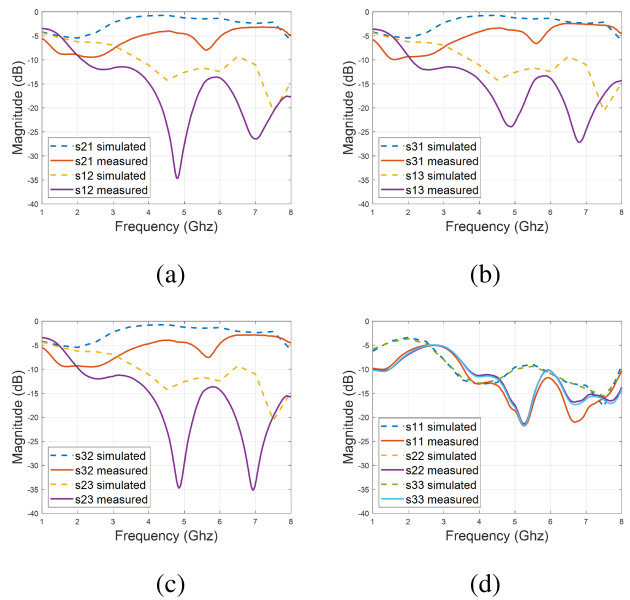


FIGURE 8. Measured S parameters of the designed circulator: (a) S21 & S12. (b) S31 & S13. (c) S32 & S23. (d) Return loss.

aligning, the air and substrate gap between the components, and the thickness of copper are considered to be ideal in the simulation.

The simulation results, which are shown in Figs. 2 and 5, indicates that by applying the broad-band impedance matching network, the impedance of the ports can be optimized to around 50 Ohm, and the measurement verifies that this method can achieve a broadband operating frequency. Nonetheless, during the measurement, one non-uniform magnetic field, which is generated by the permenet magnets, is applied to the ferrite puck, and that will introduce the differences compared to the simulation result since the performance of the ferrite material is sensitive to changes in the external magnetic field.

B. MEASUREMENTS OF THE TWIN-CIRCULATOR SIC CIRCUIT

The proposed full-duplex front-end microwave system is shown in Fig. 9. The system’s front- and back-ends consist of a 180-coupler and a splitter/combiner. The arc arrow in red color on Fig. 9 denotes the circulator’s signal circulation direction. During the measurement, the input signal at port 1 separates into 2 signals with 180° phase difference, while port b is connected to one 50 Ω load and one wide-band horn antenna, respectively. Meanwhile, the interference signals, which are the leakage signals at the twin circulators’ isolated ports, are combined at the receiver side of the full-duplex system at port c.

A wide-band coaxial 180-degree hybrid coupler that covers the frequency range of 1 to 18 GHz from SAGE Millimeter, Inc. was used for the SIC architecture measurement (left side of the SIC architecture) in order to enable a wide operating

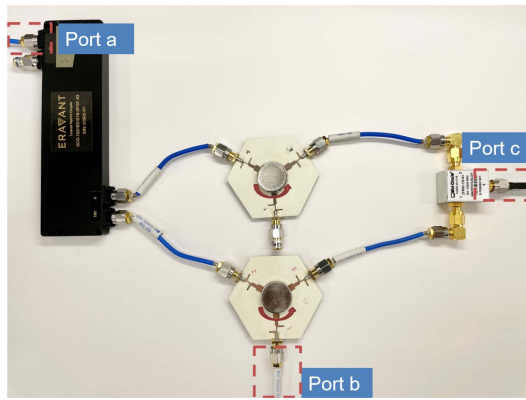


FIGURE 9. Proposed SIC architecture.

range across the full-duplex microwave system. A wideband power splitter that covers the frequency range of 1 to 12 GHz from Mini-Circuits is used in the measurement (right side of the SIC architecture).

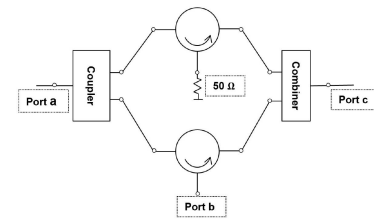
1) MEASURED S-PARAMETERS

Fig. 10 shows the measured S-parameters with a 50 Ω terminator connected at port b. Due to the transmission loss of the coupler ($\approx 3\text{--}5$ dB), the transmission loss of the circulator ($\approx 3.5\text{--}5.5$ dB), and the cable loss (≈ 1.5 dB), the overall transmission loss S_{ba} is in the range of 8–10 dB as shown in Fig. 10(d). Fig. 10(e) shows the measured losses S_{cb} around 5 dB and the maximum isolation around 30 dB at the receiver side. Compared with the interfering signal of a single circulator, which is shown in Fig. 8, Fig. 10(a) indicates that the interfering signal of the full-duplex system at the receiver side (port c) obtains a high degree of interference cancellation; the cross coupling is measured to be better than -33 dB within the frequency band from 3 to 8 GHz.

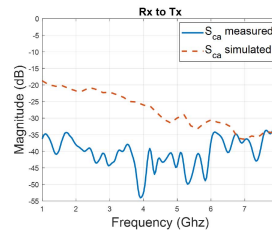
In order to evaluate the SIC system with an antenna connected, the 50 Ω terminator at port 2 is replaced with a wideband horn antenna. Fig. 11 shows the S-parameter measurement of the system with horn antenna connected at port 2. Comparing the measured return loss and interfering signal in Figs. 10 and 11, the system response is similar since the wide-band horn antenna is designed to be very well matched with 50 Ω.

2) MEASURED SIC- FROM TIME DOMAIN MEASUREMENTS

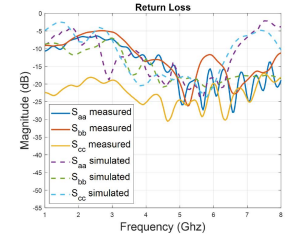
To cross-verify performance of the full-duplex front-end, we employed wideband signals in the time-domain and measured self-interference cancellation using a spectrum analysis at the receiver port. A Tektronix mixed signal oscilloscope is used to measure the frequency spectrum and time domain waveform at port b (the antenna transmit port fed by the power amplifier) and at port c (the receiver port connecting to the LNA). Meanwhile, port a is connected to the input from the signal generator to emulate the wideband signal source during the measurement.



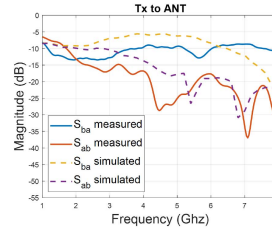
(a)



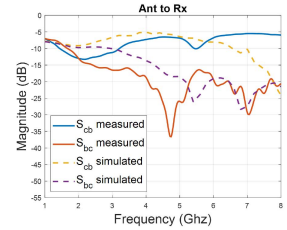
(b)



(c)

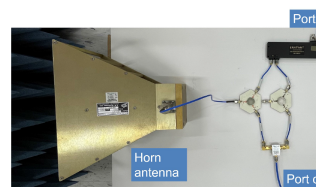


(d)

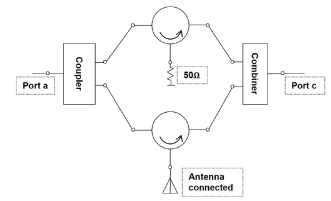


(e)

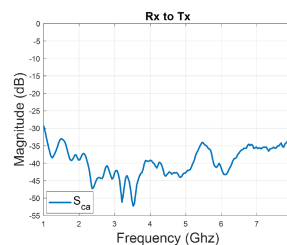
FIGURE 10. Measurement for a 50 Ω termination: (a) Designed SIC architecture. (b) Interference level at the receiver side. (c) Return loss measured at all the ports of the proposed system. (d) Signal at the transmit port showing about 10 ± 3 dB off loss. (e) Signal at the receive port showing about 5 ± 2 dB off loss.



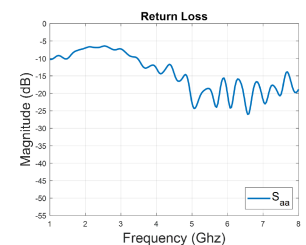
(a)



(b)



(c)



(d)

FIGURE 11. Measurement for an antenna connected at port b : (a) System with antenna connected at port b. (b) System diagram with antenna connected at port b. (c) Signal measured at the receiver side. (d) Return loss measured at port 1 of the proposed system.

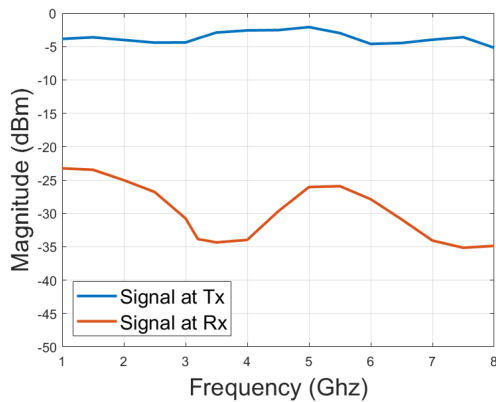


FIGURE 12. Frequency domain measurement of signal levels. The transmit signal undergoes about 3 dB of loss as measured at the Tx port. The residual self-interference at the Rx is better than -30 ± 4 dB.

Referring to the S_{ca} of the system, which is shown in Fig. 10, the interference waveform at port c maintains a low power level within the band 3 to 8 GHz. To be noticed, the signal at the Tx maintains a flat change. Therefore, the output signal at the Tx will maintain stable over 1 to 7 GHz. Although the circulator only works from 3.5 to 8 GHz, by applying the twin structure as the cancellation method, the interference signal - leakage signals with 180 phase difference - at Rx will cancel each other and thus still remains in low power from 3 to 8 GHz.

Fig. 12 shows the signal power measurement at port b and port c for the frequency band 1 to 8 GHz by applying the RF signal at port a from the RF signal generator. The measured signal at the transmit side-Tx-is marked in blue curve, and the leaking signal at the interference port-Rx-is marked in red. The best isolation performance for the proposed system is from 3 to 8 GHz due to the best operating frequency range of the circulator. The measured transmitted signal at the transmit port is -3 dBm and the measured interfering signal at the receiver side is -33 dBm. The proposed system achieves an isolation better than 30 dB over a wide bandwidth from 3 to 8 GHz.

V. CONCLUSION

We proposed and fabricated an RF front-end system for in-band full-duplex (IBFD) communications using a linear and time-invariant system obtained using a coupler, a power divider and a pair of circulators. The fabricated and tested full-duplex allows STAR applications across the 3–8 GHz band using a RF systems approach. We proposed and fabricated an ultra-wideband ferrite based circulator design; this circulator forms the building block of the STAR system for IBFD radio. Measurements show that the fabricated circulator maintains a high isolation of around 30 dB, and a broad bandwidth from 3 GHz to 8 GHz was obtained. Compared with other ferrite based microstrip circulator designs, the proposed circulator design achieves a wider bandwidth and a higher isolation within the 3–8 GHz band. High self-interference

(SI) cancellation is then achieved by introducing the building block circulators, couplers and splitters in the proposed IBFD system. Furthermore, a physically symmetrical structure was proposed and tested to better isolate and reduce the SI signal in the IBFD system. Compared with other IBFD systems, our proposed IBFD microwave system achieves more than 25 dB cancellation (isolation) of the SI signal over a relatively ultra-wide band from 3 to 8 GHz by using two circulators that individually only operate in the 3–8 GHz band. However, the losses in our experimental system was significant. The lossy nature of the circulators used in the experiment has been taken into account in metric M_2 . The use of optimized circulators from commercial sources which have low loss (typically less than 0.5 dB) can be considered for real world applications. The differential cancellation of reflections used in the proposed structure allows higher tolerance of impedance mismatches across the 3–8 GHz range. This leads to a bandwidth extension as well as improved circulation system-wide. In a sense, the proposed system achieves wideband STAR performance at the cost of higher system losses.

REFERENCES

- [1] H. Zhao et al., "A broadband multistage self-interference canceller for full-duplex MIMO radios," *IEEE Trans. Microw. Theory Techn.*, vol. 69, no. 4, pp. 2253–2266, Apr. 2021.
- [2] T. Chen et al., "A survey and quantitative evaluation of integrated circuit-based antenna interfaces and self-interference cancellers for full-duplex," *IEEE Open J. Commun. Soc.*, vol. 2, pp. 1753–1776, 2021.
- [3] L. Laughlin, M. A. Beach, K. A. Morris, and J. L. Haine, "Optimum single antenna full duplex using hybrid junctions," *IEEE J. Sel. Areas Commun.*, vol. 32, no. 9, pp. 1653–1661, Sep. 2014.
- [4] M. Mikhael, B. van Liempd, J. Craninckx, R. Guindi, and B. Debaillie, "An in-band full-duplex transceiver prototype with an in-system automated tuning for RF self-interference cancellation," in *Proc. IEEE 1st Int. Conf. 5G Ubiquitous Connectivity*, 2014, pp. 110–115.
- [5] L. Laughlin, M. A. Beach, K. A. Morris, and J. L. Haine, "Electrical balance duplexing for small form factor realization of in-band full duplex," *IEEE Commun. Mag.*, vol. 53, no. 5, pp. 102–110, May 2015.
- [6] T. Vermeulen, M. Laghate, G. Hattab, B. van Liempd, D. Cabric, and S. Pollin, "Nearly instantaneous collision and interference detection using in-band full duplex," in *Proc. IEEE Int. Symp. Dyn. Spectr. Access Netw.*, 2017, pp. 1–2.
- [7] T. Vermeulen, B. van Liempd, B. Hershberg, and S. Pollin, "Real-time RF self-interference cancellation for in-band full duplex," in *Proc. IEEE Int. Symp. Dyn. Spectr. Access Netw.*, 2015, pp. 275–276.
- [8] G. Qi, B. van Liempd, P.-I. Mak, R. P. Martins, and J. Craninckx, "A SAW-less tunable RF front end for FDD and IBFD combining an electrical-balance duplexer and a switched-LC n-path LNA," *IEEE J. Solid-State Circuits*, vol. 53, no. 5, pp. 1431–1442, May 2018.
- [9] B. van Liempd, A. Visweswaran, S. Ariumi, S. Hitomi, P. Wambacq, and J. Craninckx, "Adaptive RF front-ends using electrical-balance duplexers and tuned SAW resonators," *IEEE Trans. Microw. Theory Techn.*, vol. 65, no. 11, pp. 4621–4628, Nov. 2017.
- [10] L. Laughlin, C. Zhang, M. A. Beach, K. A. Morris, and J. L. Haine, "Electrical balance duplexer field trials in high-speed rail scenarios," *IEEE Trans. Antennas Propag.*, vol. 65, no. 11, pp. 6068–6075, Nov. 2017.
- [11] E. Manuzato, J. Tamminen, M. Turunen, D. Korpi, F. Granelli, and M. Valkama, "Digitally-controlled electrical balance duplexer for transmitter-receiver isolation in full-duplex radio," in *Proc. IEEE 22nd Eur. Wireless Conf.*, 2016, pp. 1–8.
- [12] S. Khaledian, F. Farzami, B. Smida, and D. Erricolo, "Inherent self-interference cancellation for in-band full-duplex single-antenna systems," *IEEE Trans. Microw. Theory Techn.*, vol. 66, no. 6, pp. 2842–2850, Jun. 2018.

- [13] S. K. Cheung, W. H. Weedon, and C. P. Caldwell, "High isolation lange-ferrite circulators with NF suppression for simultaneous transmit and receive," in *Proc. IEEE MTT-S Int. Microw. Symp.*, 2010, pp. 1352–1355.
- [14] C. Xu, E. Calayir, and G. Piazza, "Magnetic-free electrical circulator based on ALN MEMS filters and CMOS RF switches," in *Proc. IEEE Micro Electro Mech. Syst.*, 2018, pp. 755–758.
- [15] N. Reiskarimian, J. Zhou, and H. Krishnaswamy, "A CMOS passive LPTV nonmagnetic circulator and its application in a full-duplex receiver," *IEEE J. Solid-State Circuits*, vol. 52, no. 5, pp. 1358–1372, May 2017.
- [16] S. Jain, A. Agrawal, M. Johnson, and A. Natarajan, "A 0.55-to-0.9 GHz 2.7 dB NF full-duplex hybrid-coupler circulator with 56 MHz 40 dB TX SI suppression," in *Proc. IEEE Int. Solid-State Circuits Conf.*, 2018, pp. 400–402.
- [17] A. Nagulu, A. Alù, and H. Krishnaswamy, "Fully-integrated non-magnetic 180 nm SOI circulator with > 1 W P1dB, > 50 dBm IIP3 and high isolation across 1.85 VSWR," in *Proc. IEEE Radio Freq. Integ. Circuits Symp.*, 2018, pp. 104–107.
- [18] T. Dinc, A. Nagulu, and H. Krishnaswamy, "A millimeter-wave non-magnetic passive SOI CMOS circulator based on spatio-temporal conductivity modulation," *IEEE J. Solid-State Circuits*, vol. 52, no. 12, pp. 3276–3292, Dec. 2017.
- [19] A. M. Darwish et al., "Multi-octave GAN MMIC circulator for simultaneous transmit receive applications," in *Proc. IEEE/MTT-S Int. Microw. Symp.*, 2018, pp. 417–419.
- [20] U. De Silva, H. Malavipathirana, S. Pulipati, S. Bhardwaj, S. Mandal, and A. Madanayake, "Implementation and testing of a switching circulator for twin-pair STAR radio architectures," in *Proc. Moratuwa Eng. Res. Conf.*, 2020, pp. 331–336.
- [21] S. K. Cheung, T. P. Halloran, W. H. Weedon, and C. P. Caldwell, "MMIC-based quadrature hybrid quasi-circulators for simultaneous transmit and receive," *IEEE Trans. Microw. Theory Techn.*, vol. 58, no. 3, pp. 489–497, Mar. 2010.
- [22] W. H. Tranter and R. E. Ziemer, *Principles of COMMUNICATIONS-Systems, Modulation, and Noise*. Hoboken, NJ, USA: Wiley, 2014.
- [23] U. D. Silva, S. Pulipati, S. B. Venkatakrishnan, S. Bhardwaj, and A. Madanayake, "A passive star microwave circuit for 1-3 GHz self-interference cancellation," in *Proc. IEEE 63rd Int. Midwest Symp. Circuits Syst.*, 2020, pp. 105–108.
- [24] H. Bosma, "On stripline y-circulation at UHF," *IEEE Trans. Microw. Theory Techn.*, vol. 12, no. 1, pp. 61–72, Jan. 1964.
- [25] E. Skomal, "Theory of operation of a 3-port y-junction ferrite circulator," *IEEE Trans. Microw. Theory Techn.*, vol. 11, no. 2, pp. 117–122, Mar. 1963.
- [26] B. Peng, W. Zhang, Y. Sun, J. Lin, W. Zhang, and H. Li, "Design of microstrip y-junction circulator based on ferrite thin films," in *Proc. IEEE China-Jpn. Joint Microw. Conf.*, 2011, pp. 1–4.
- [27] V. Kelaiya and M. R. Naik, "Design and simulation of x band microstrip circulator," in *Proc. IEEE Region 10 Conf.*, 2016, pp. 1961–1964.
- [28] A. Borjak and L. Davis, "More compact ferrite circulator junctions with predicted performance," *IEEE Trans. Microw. Theory Techn.*, vol. 40, no. 12, pp. 2352–2358, Dec. 1992.
- [29] A. Ashley, L. F. Marzall, M. Pinto, Z. Popovic, and D. Psychogiou, "Bandwidth design of ferrite-based circulators," in *Proc. IEEE Int. Appl. Comput. Electromagnetics Soc. Symp.*, 2018, pp. 1–2.
- [30] M. Pinto, L. Marzall, A. Ashley, D. Psychogiou, and Z. Popović, "Design-oriented modelling of microstrip ferrite circulators," in *Proc. IEEE 48th Eur. Microw. Conf.*, 2018, pp. 215–218.
- [31] C. Weil, T. Hauck, J. Schur, and J. Müller, "Broadband Ku- And ka-band circulators in LTCC using sintered bulk ferrites," in *Proc. IEEE 51st Eur. Microw. Conf.*, 2022, pp. 18–21.
- [32] H.-W. Chao, S. Y. Wu, and T.-H. Chang, "Bandwidth broadening for stripline circulator," *Rev. Sci. Instrum.*, vol. 88, no. 2, 2017, Art. no. 024706.
- [33] V. Olivier et al., "Stripline dual-band ferrite circulators operating on weak field conditions," in *Proc. IEEE 50th Eur. Microw. Conf.*, 2021, pp. 860–863.
- [34] H. Turki, L. Huitema, T. Monediere, B. Lenoir, and C. Breuil, "Complete methodology of low-loss ultra-wideband junction circulator," in *Proc. IEEE/MTT-S Int. Microw. Symp.*, 2018, pp. 746–749.
- [35] H. Dong, "Broad-band and high-isolation performance of a lumped-element circulator: Theory and experiment," Ph.D. dissertation, Univ. Idaho, Moscow, ID, USA, 2014.
- [36] J. R. Smith, H. Dong, J. L. Young, and B. Aldecoa, "Optimization of a broadband VHF lumped-element ferrite circulator," *Microw. Opt. Technol. Lett.*, vol. 55, no. 7, pp. 1476–1481, 2013.
- [37] A. Ashley and D. Psychogiou, "Rf co-designed bandpass filter/circulator with tunable center frequency, bandwidth, and out-of-band isolation," *IEEE Microw. Wireless Compon. Lett.*, vol. 31, no. 7, pp. 845–848, Jul. 2021.
- [38] J. L. Young, R. S. Adams, B. O'Neil, and C. M. Johnson, "Bandwidth optimization of an integrated microstrip circulator and antenna assembly: Part 1," *IEEE Antennas Propag. Mag.*, vol. 48, no. 6, pp. 47–56, Dec. 2006.
- [39] J. L. Young, R. S. Adams, B. O'Neil, and C. Johnson, "Bandwidth optimization of an integrated microstrip circulator and antenna assembly: Part 2," *IEEE Antennas Propag. Mag.*, vol. 49, no. 1, pp. 82–91, Feb. 2007.
- [40] S. Ayter and Y. Ayasli, "The frequency behavior of stripline circulator junctions," *IEEE Trans. Microw. Theory Techn.*, vol. 26, no. 3, pp. 197–202, Mar. 1978.
- [41] C. Multiphysics, "Three-port waveguide ferrite circulator," Jul. 2022. [Online]. Available: <https://www.comsol.com/model/download/823871/models.rf.circulator.pdf>
- [42] D. M. Pozar, *Microwave Engineering*. Hoboken, NJ, USA: Wiley, 2011.